Measurements of Thermal Accommodation Coefficients

W. M. Trott[*], D. J. Rader[*], J. R. Torczynski[*], J. N. Castañeda[*], M. A. Gallis[*], and L. A. Gochberg[†]

[*]*Engineering Sciences Center, Sandia National Laboratories, Albuquerque, New Mexico 87185 USA*
[†]*Novellus Systems, Inc., 4000 North First Street, San Jose, California 95134 USA*

Abstract. An experimental apparatus is described for measuring gas-surface thermal accommodation coefficients based on the pressure dependence of the conductive heat flux between parallel plates separated by a gas-filled gap. The heat flux is inferred from measurements of the temperature difference between the plate surface and an adjacent temperature-controlled water bath. The apparatus can be used with a variety of gases (e.g., monatomic, diatomic, polyatomic, mixtures) in contact with surfaces of different materials (e.g., metals, semiconductors, insulators) with different surface finishes (e.g., smooth, rough). Experiments are reported for nitrogen, argon, and helium in contact with pairs of 304 stainless steel plates having either machined or polished finishes. The thermal accommodation coefficients for nitrogen and argon with machined and polished 304 stainless steel plates do not depend on the finish to within the experimental uncertainty: 0.80±0.02 for nitrogen and 0.87±0.02 for argon. The values for helium are much lower and show a slight variation with finish: 0.36±0.02 for the machined finish and 0.40±0.02 for the polished finish.

INTRODUCTION

Heat transfer between solid surfaces and noncontinuum gas flows continues to be an active area of research. Noncontinuum effects arise when the system length scale L is comparable to or smaller than the molecular mean free path λ. Here, Springer's definition [1] is used: $\lambda = 2\mu/\rho\bar{c}$, where μ is the gas viscosity, ρ is the gas mass density, $\bar{c} = (8k_B T/\pi m)^{1/2}$ is the mean molecular speed, T is the gas temperature, m is the gas molecular mass, and $k_B = 1.380658\times10^{-23}$ J/K is the Boltzmann constant.

Micron-scale applications have become more common since the advent of Micro Electro Mechanical Systems (MEMS). Examples include microscale thermal actuators (see Figure 1), in which beams heated by electrical current are separated from the substrate by micron-scale gas-filled gaps [2]. Such devices usually operate in ambient air, for which $\lambda \approx 0.065$ μm [3]. Thus, microscale gas-phase heat conduction exhibits noncontinuum features.

An experimentally-validated database of gas-surface interaction models is required to predict noncontinuum gas-phase heat fluxes. Unfortunately, reliable gas-surface interaction models are lacking for many microsystem materials at typical conditions. For example, Yang and Bennett [4] report molecular-beam measurements of the thermal accommodation coefficient for nitrogen reflecting from single-crystal silicon and polyimide surfaces. However, the temperatures in their study (1650 K) are much higher than typical microsystem temperatures.

A major step toward meeting this need is the development of an experimental apparatus for measuring gas-surface thermal accommodation coefficients [5,6]. Such an apparatus is described below, and initial experiments are reported for nitrogen, argon, and helium in contact with pairs of 304 stainless steel plates with either a standard-machined (lathe) finish or a mirror-polished finish.

GAS-SURFACE INTERACTIONS

Heat transfer between solid surfaces and noncontinuum gas flows continues to be investigated since Maxwell's pioneering work over 100 years ago [7]. Despite considerable effort in this area, models for detailed gas-surface interaction mechanisms are still lacking [8]. In their absence, theoretical predictions can usually be brought into agreement with experimental observations by using empirical accommodation-coefficient models. The thermal

accommodation coefficient is defined as $\alpha = (E_{in} - E_{re})/(E_{in} - E_w)$, where E_{in} is the incident energy flux, E_{re} is the reflected energy flux, and E_w is the reflected energy flux obtained if the molecules are in thermal equilibrium with the surface [1,9]. The partition of reflections into a diffuse, fully accommodated fraction α and a specular fraction $(1-\alpha)$ is referred to as the Maxwell model. Although one recent experimental study reports translational and rotational thermal accommodation coefficients for certain gases in contact with tungsten [10], studies that separate contributions from the different energy modes for other gas-surface combinations are not common [11].

Previous experimental studies have measured the thermal accommodation coefficient in a variety of geometries and over a wide range of gas-surface combinations [1,11]. The data show that accommodation depends on the composition and the temperature of the gas and the surface, on the gas pressure, and on the state of the surface (roughness, contaminant adsorption, gas adsorption). Experimental values range from 0.01 to nearly unity. The smaller values are observed for lower-molecular-weight gases striking clean surfaces (e.g., helium on tungsten [10]). Near-unity values are observed for higher-molecular-weight gases striking contaminated or roughened surfaces (e.g., xenon on platinum [11]). However, data for recently-developed industrial and microsystem surfaces are lacking.

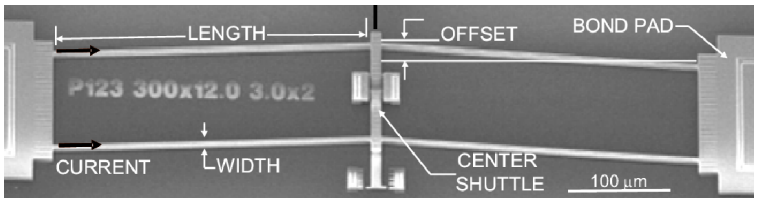

FIGURE 1. Microscale thermal actuator: white, beams; gray, substrate [2].

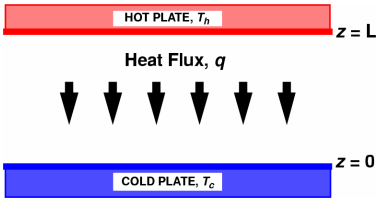

FIGURE 2. Fourier geometry.

PARALLEL-PLATE HEAT TRANSFER

In this study, the thermal accommodation coefficient is inferred from the pressure dependence of heat flux across a gas-filled gap between two parallel disks of unequal temperature. This finite geometry is related to the Fourier problem, in which a quiescent gas occupies a gap of height L between two infinite parallel plates at unequal temperatures, as shown in Figure 2. The coordinate system is defined such that $z = 0$ and $z = L$ correspond to the surfaces of the bottom and top plates, respectively. The temperature of the top plate, T_h, is slightly higher than that of the lower plate, T_c, although the temperature difference here is small: $T_h - T_c << T_c$. Since the gas is quiescent (no mass flow), the gas-phase heat transfer between the plates is dominated by conduction: convection is negligible, and radiation is small although not negligible. The Maxwell gas-surface interaction model [7] is considered, as discussed above. Here, the experiments are performed with the same materials and surface finishes for both plates, so both plates are taken to have the same value of the thermal accommodation coefficient α.

When $T_h - T_c << T_c$, the heat flux in the Fourier geometry is known exactly both in the free-molecular limit (q_{FM}, for $\lambda >> L$) [12] and in the continuum limit (q_C, for $\lambda << L$):

$$q_{FM} = -\frac{1}{2}\left(\frac{P\bar{c}}{T}\right)\left(\frac{\alpha}{2-\alpha}\right)\left(1+\frac{\zeta}{4}\right)(T_h - T_c), \qquad q_C = -K\left(\frac{T_h - T_c}{L}\right), \tag{1}$$

where K is the gas thermal conductivity and ζ is the number of internal energy modes (0 for argon and helium, and 2 for ambient nitrogen). Thus, q_{FM} is proportional to P, whereas q_C is independent of P.

Although many theoretical analyses are available in the literature [1], few predictions of the heat flux in the transitional regime result in closed-form expressions. One exception is Liu and Lees [13], who use a four-moment solution of the linearized Boltzmann equation for a monatomic gas to derive an approximate expression. Springer [1] extends this analysis to polyatomic gases for small temperature differences, equal wall thermal accommodation coefficients, and arbitrary gas pressures. Springer [1] shows that this expression agrees reasonably well with the available experimental data for monatomic and diatomic gases over a wide range of conditions. Independently, Sherman [14] presents a similar but slightly more general expression. The Sherman-Lees equation is given below in two forms, where the second form is the more convenient one for analyzing experimental results:

$$\frac{q}{q_C} = \frac{q_{FM}}{q_{FM} + q_C}, \qquad \frac{1}{q} = \frac{1}{q_C} + \frac{1}{q_C}\cdot\frac{2KT}{L(\alpha/(2-\alpha))(1+(\zeta/4))\bar{c}}\cdot\frac{1}{P}. \tag{2}$$

EXPERIMENTAL APPARATUS

The experimental apparatus used in this study [5,6] is shown in Figure 3. A vacuum test chamber contains the systems and diagnostics required for heat-flux measurements between two parallel, 142.5-mm-diameter plates separated by ~10-mm gas-filled gaps. To provide a high degree of accuracy, state-of-the-art components are used to control plate alignment, plate positions, plate temperatures, gas temperature, gas pressure, and gas flow rate.

A schematic diagram of the test chamber cross section is also shown in Figure 3. The test chamber is a 410-mm-diameter sphere with six 336.6-mm (13.25-inch) OD standard conflat flanges (Varian) mounted symmetrically. The opposing upper and lower flanges are used to mount the upper and lower plate assemblies. An observation window (optical-quality quartz) occupies the flange extending out of plane, while a cryogenic pump occupies the flange extending into the plane. Separate chambers house an electron gun for gas density measurements using electron beam fluorescence [5]; measurements with this device are reported elsewhere [5].

Stable control and accurate measurement of gas conditions in the test chamber are essential. Pressure measurements are made using five MKS 690A high-accuracy Baratron pressure transducers (0.05% of full scale). An MKS 244E pressure/flow controller maintains the desired chamber pressure by regulating the gas flow with an automated MKS 245 proportioning control valve. Tests show that the flow controller provides highly stable chamber pressures. For example, the system can maintain a pressure of 30.00±0.01 mTorr over long periods of operation.

The assemblies that hold the test plates (whose working surfaces are in contact with the gas and define the gas-surface interface) are designed to meet several aggressive requirements: 1) maintain a constant temperature across the test plate surface, 2) precisely position each plate independently, 3) maintain parallel alignment between the two plates, 4) provide thermistor access for heat-flux measurements, and 5) allow for ~1-day interchange of plates.

To provide interchangeability, the test plates are fabricated from commercially-available 6-inch conflat flanges. The experiments here use 25.4-mm-thick, 304 stainless steel conflat flanges reduced to a 142.7-mm OD. Each plate is attached to a flanged plenum, or "spool", that provides contact between a 0.62-liter temperature-controlled water bath and the plate's back side. Three high-precision Hart Scientific thermistors (±0.01°C accuracy, 0.005°C repeatability) are embedded to within ~1.6 mm of the surface of each plate: one thermistor is centered, while the other two are positioned at a radius of 38 mm (1.5 inch). Another thermistor is submerged within the water bath of each spool. The embedded thermistors measure the plate temperature and check for uniformity, while the difference between the centered embedded thermistor and the submerged bath thermistor is used to infer heat flux. It is the high precision of the thermistors that enables heat-flux measurements of the required accuracy.

The plate/spool assemblies are mounted to extension columns (see Figure 3) with extensible metal bellows that seal to the top and bottom flanges of the test chamber. The vertical position of each assembly is controlled by a separate Thermionics precision positioner. These positioners can adjust the vertical position of the ~20-kg plate/spool assemblies with ~10-μm accuracy. Software controls the position of each assembly independently but can also operate the two positioners in a master/slave mode to maintain a fixed distance between the plates.

Tests are performed on pairs of 304 stainless steel plates with one of two surface finishes. The first pair has a standard-machined (rough) finish with an RMS roughness of ~2 μm, and the second pair has a mirror-polished (smooth) finish with an RMS roughness of ~0.02 μm—a hundredfold reduction in surface roughness. The thermal accommodation coefficients of these two pairs of plates with nitrogen, argon, and helium are presented below.

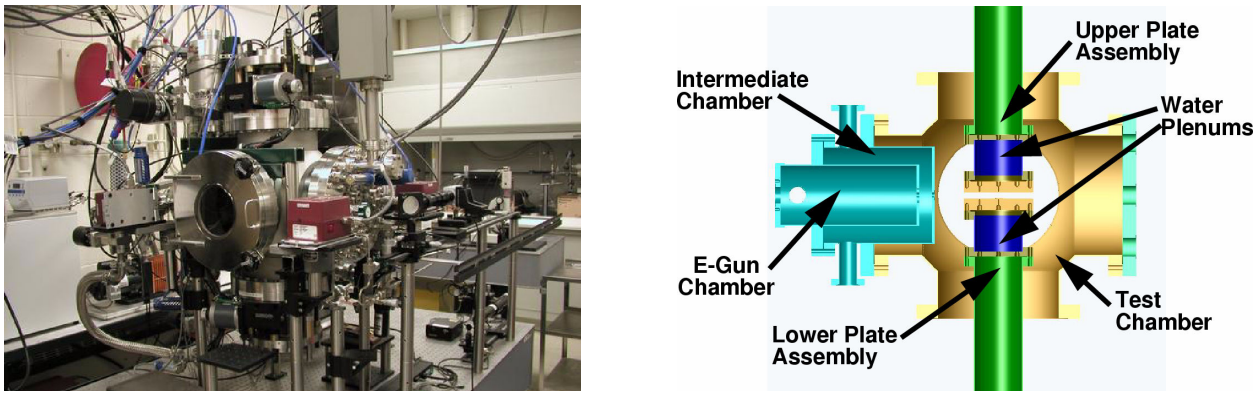

FIGURE 3. Left: photograph of the test apparatus. Right: schematic diagram of the vacuum chamber cross section.

THERMAL-ACCOMMODATION-COEFFICIENT MEASUREMENTS

The following approach is used to determine the thermal accommodation coefficient. First, the total temperature difference between the centered-plate and bath thermistors is measured as a function of the gas pressure for fixed plate conditions. This measurement is complicated by the fact that solid and liquid thermal conductivities are very large compared to those of gases, producing small temperature differences. Next, the parasitic heat losses that are always present in the system are subtracted from the total heat flux: a nonzero heat flux results from radiation and solid conduction in the absence of gas (vacuum). At a nonzero pressure, the temperature difference caused by gas-phase conduction, ΔT_{gas}, is determined by subtracting the temperature difference observed under vacuum, ΔT_{rad}, caused by radiation and solid conduction, from the observed temperature difference, ΔT: $\Delta T_{gas} = \Delta T - \Delta T_{rad}$. Radiation is much smaller than gas-phase conduction at higher pressures but becomes important at low pressures. Finally, the limiting value of the continuum heat flux at high pressures is used as a calibration point. Thus, with the assumption that the measured gas temperature difference is proportional to the heat flux, the following expressions describe the heat flux and the gas-phase contribution to the temperature difference at arbitrary pressures:

$$\frac{q}{q_C} = \frac{\Delta T_{gas}}{\Delta T_C}, \qquad \frac{1}{\Delta T_{gas}} = \frac{1}{\Delta T_C} + \frac{1}{\Delta T_C} \cdot \frac{2KT}{L\left(\frac{\alpha}{2-\alpha}\right)\left(1+\frac{\zeta}{4}\right)\bar{c}} \cdot \frac{1}{P}. \tag{3}$$

The above expressions are based on two assumptions: 1) that the measured temperature differences are linearly related to the heat flux, and 2) that the Sherman-Lees equation exactly describes the pressure dependence of the heat flux. Nevertheless, the second expression above is used to correlate the experimental results. Its form suggests that a plot of $1/\Delta T_{gas}$ against $1/P$ should be linear. A graphical interpretation of such a plot is that the intercept equals $1/\Delta T_C$ and that the slope is a function of known quantities and the thermal accommodation coefficient. Thus, a linear regression can be used to determine a best-fit value for the slope, from which the thermal accommodation coefficient α is extracted [5,6].

An example of this procedure is shown in Figure 4. The left plot shows the temperature-difference history for nitrogen in contact with the hot machined 304 stainless steel plate for a gap of 5 mm and bath temperatures of 15°C and 35°C. The temperature-difference history for the cold plate is similar and therefore is not shown. Thermistor readings are recorded with the chamber held at vacuum and at pressures between 1 and 6700 mTorr. Radiation heat losses are clearly evident for the 0-mTorr case, from which it is inferred that $\Delta T_{rad} = 0.026°C$. At large pressures, the temperature difference approaches a limiting value: $\Delta T_{gas} \rightarrow \Delta T_C = 0.190°C$. The right plot of this figure shows the inverse gas temperature difference plotted against the inverse gas pressure for both plates under these conditions. Also shown are the best-fit versions of the above equation to the experimental values, which correspond to thermal accommodation values of 0.808 and 0.795 for the cold and hot plates, respectively. The difference between these values is comparable to their uncertainty, ±0.02. Moreover, the linear form represents the experimental values well.

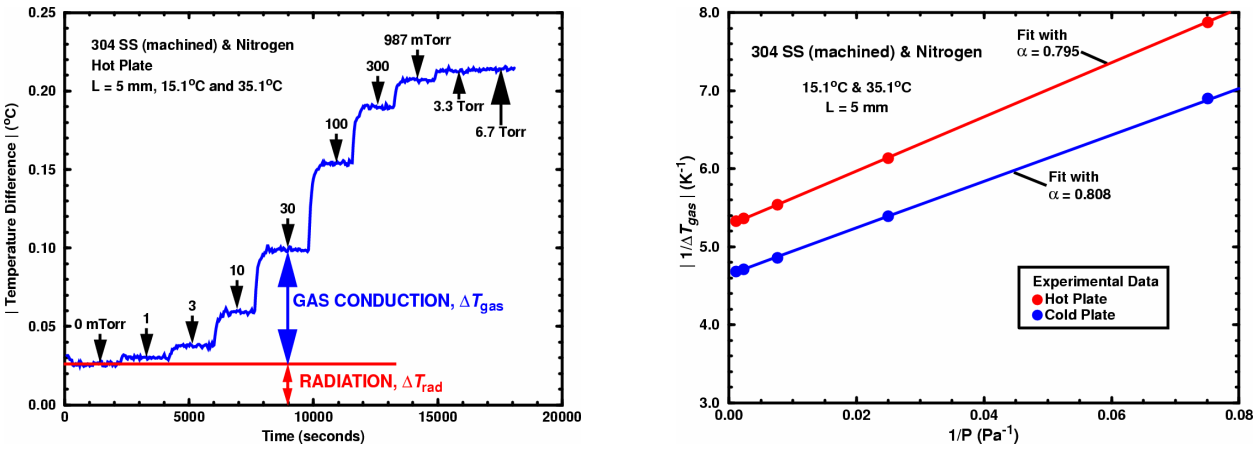

FIGURE 4. Temperature difference vs. gas pressure: nitrogen, machined 304 stainless steel, hot plate, 5-mm gap. Left: plotted as history. Right: plotted with fits to determine thermal accommodation coefficients.

EXPERIMENTAL RESULTS

Measurements of ΔT_{gas} as a function of P are made with pairs of machined (RMS roughness of ~2 μm) and polished (RMS roughness of ~0.02 μm) 304 stainless steel plates in contact with nitrogen, argon, and helium [5,6]. For each gas-plate combination, tests are performed using several combinations of plate separation and hot and cold temperatures. The data are analyzed as above to determine the thermal accommodation coefficient. As in Figure 4, good linear fits are obtained in all cases (typically $r^2 \approx 0.99999$). All experimental conditions and results are summarized in Table 1.

The thermal accommodation coefficients for cold and hot plates are typically in very good agreement. For example, the values with machined cold and hot plates are 0.808 and 0.795 for nitrogen, 0.875 and 0.866 for argon, and 0.363 and 0.360 for helium, respectively. As expected, the thermal accommodation coefficient is seen to decrease with decreasing gas molecular weight. Based on these and additional tests, the best-estimate thermal accommodation coefficients for nitrogen, argon, and helium in contact with machined (rough) 304 stainless steel are 0.80±0.02, 0.87±0.02, and 0.36±0.02, respectively.

The left plot of Figure 5 shows data for nitrogen with the machined and polished cold plates. Hot-plate results are almost identical to cold-plate results, and argon results are qualitatively similar to nitrogen results, so these results are not shown. The machined and polished curves are nearly parallel, implying that the thermal accommodation coefficients are almost the same. Similar behavior is observed for the machined and polished cold plates with argon. The best estimates of the thermal accommodation coefficients for argon and nitrogen in contact with the polished plates (taken as the average of the hot-plate and cold-plate values) are 0.87±0.02 and 0.80±0.02, respectively. Thus, the thermal accommodation coefficients for the machined and polished plates agree to within experimental uncertainty for both gases.

The right plot of Figure 5 also shows cold-plate data for helium with the machined and polished plates. The helium results are different from the nitrogen and argon results in that the two slopes are clearly distinguishable, implying slightly different thermal accommodation coefficients for the two different finishes. The best estimate of the thermal accommodation coefficient for helium in contact with the polished plates is 0.40±0.02. Thus, there is a small increase (comparable to the uncertainty) in accommodation with decreasing surface roughness for helium and 304 stainless steel. The fact that decreasing the surface roughness by a factor of ~100 either does not change the thermal accommodation coefficient or produces a very slight increase is somewhat unexpected since roughness is generally thought to increase accommodation.

TABLE 1. Gases, experimental conditions, and thermal accommodation coefficients with 304 stainless steel plates.

Gas	Gap	Cold Temp.	Hot Temp.	Pressure	Machined	Polished
Nitrogen	5 mm	15.1°C	35.1°C	4-900 Pa	0.80±0.02	0.80±0.02
Argon	10 mm	5.2°C	45.0°C	6-1400 Pa	0.87±0.02	0.87±0.02
Helium	10 mm	20.2°C	30.1°C	25-1400 Pa	0.36±0.02	0.40±0.02

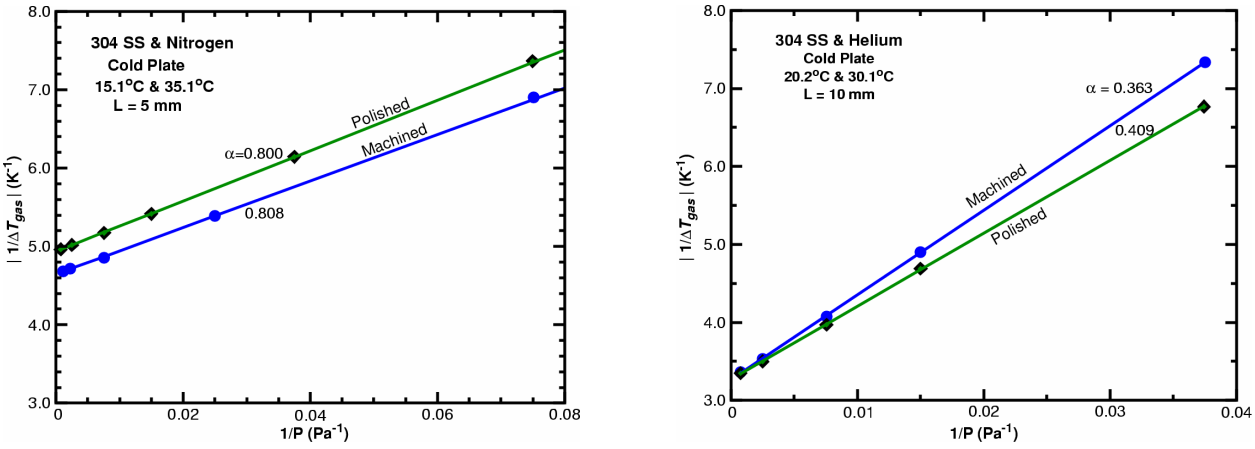

FIGURE 5. Temperature difference vs. pressure with thermal-accommodation-coefficient fits. Left: nitrogen. Right: helium.

CONCLUSIONS

A priori prediction of noncontinuum, gas-phase heat flux requires a detailed description of the gas-surface interaction. Because of the physical complexity of the problem, the most effective approach to providing such descriptions involves careful experimental investigations. Unfortunately, experimental data are lacking for the materials and finishes encountered in modern industrial applications, e.g. semiconductor manufacturing and MEMS. This study reports on the development of an experimental apparatus and diagnostics that can provide precise measurements of gas-surface thermal accommodation coefficients for the materials and finishes of current interest.

As a demonstration of this new capability, thermal accommodation coefficients are reported for nitrogen, argon, and helium in contact with pairs of 304 stainless steel plates prepared with standard-machined or mirror-polished finishes. The measured accommodation coefficients for nitrogen and argon in contact with these two finishes are indistinguishable within experimental uncertainty. Thus, the accommodation coefficients of 304 stainless steel with nitrogen and argon are 0.80±0.02 and 0.87±0.02, respectively, independent of surface roughness. The thermal accommodation coefficient of helium has a slight variation with 304 stainless steel surface roughness: 0.36±0.02 for a machined finish and 0.40±0.02 for a polished finish. Future plans include tests with microsystem materials such as silicon, silicon dioxide, and gold, and industrially-relevant materials such as aluminum and alumina ceramic.

ACKNOWLEDGMENTS

This work was performed at Sandia National Laboratories. Sandia is a multiprogram laboratory operated by Sandia Corporation, a Lockheed Martin Company, for the United States Department of Energy's National Nuclear Security Administration under contract DE-AC04-94AL85000.

REFERENCES

1. G. S. Springer, "Heat Transfer in Rarefied Gases," in *Advances in Heat Transfer*, edited by T. F. Irvine and J. P. Hartnett, Academic Press, New York (1971), pp. 163-218.
2. M. A. Gallis, J. R. Torczynski, and D. J. Rader, "A Computational Investigation of Noncontinuum Gas-Phase Heat Transfer between a Heated Microbeam and the Adjacent Ambient Substrate," *Sensors and Actuators A*, in press (2006).
3. G. E. Karniadakis and A. Beskok, *Micro Flows: Fundamentals and Simulation,* Springer-Verlag, New York (2002).
4. H. Yang and T. D. Bennett, "Time of Flight Measurements of Thermal Accommodation Coefficient," Paper NHTC2000-12035, ASME International, New York (2000).
5. D. J. Rader, W. M. Trott, J. R. Torczynski, M. A. Gallis, J. N. Castañeda, and T. W. Grasser, *Microscale Rarefied Gas Dynamics and Surface Interactions for EUVL and MEMS Applications*, Report SAND2004-5329, Sandia National Laboratories, Albuquerque (2004).
6. D. J. Rader, W. M. Trott, J. R. Torczynski, J. N. Castañeda, and T. W. Grasser, *Measurements of Thermal Accommodation Coefficients*, Report SAND2005-6084, Sandia National Laboratories, Albuquerque (2005).
7. J. C. Maxwell, *The Scientific Papers of James Clerk Maxwell*, Volume 2, Cambridge University Press, London (1890).
8. T. Ohwada, "Heat Flow and Temperature and Density Distributions in a Rarefied Gas between Parallel Plates with Different Temperatures," *Physics of Fluids,* **8** (8), 2153-2160 (1996).
9. S. A. Schaaf and P. L. Chambre, "Flow of Rarefied Gases," in *Fundamentals of Gasdynamics*, Volume 3, edited by H. W. Emmons, Princeton University Press, Princeton (1958), pp. 687-739.
10. A. K. Rebrov, A. A. Morozov, M. Yu. Plotnikov, N. I. Timoshenko, and A. V. Shishkin, "Using a Thin Wire in a Free-Molecular Flow for Determination of Accommodation Coefficients of Translational and Internal Energy," in *Rarefied Gas Dynamics: 23rd International Symposium*, edited by A. D. Ketsdever and E. P. Muntz, American Institute of Physics, Melville (2003), pp. 1016-1021.
11. S. C. Saxena and R. K. Joshi, *Thermal Accommodation and Adsorption Coefficients of Gases*, Hemisphere Publishing Company, New York (1989).
12. G. A. Bird, *Molecular Gas Dynamics and the Direct Simulation of Gas Flows*, Clarendon Press, Oxford (1994), p. 84.
13. C. Y. Liu and L. Lees, "Kinetic Theory Description of Plane Compressible Couette flow," in *Rarefied Gas Dynamics*, edited by L. Talbot, Academic Press, New York (1961), pp. 391-428.
14. F. S. Sherman, "A Survey of Experimental Results and Methods for the Transition Regime of Rarefied Gas Dynamics," in *Rarefied Gas Dynamics,* Volume II, edited by J. A. Lauermann, Academic Press, New York (1963), pp. 228-260.